

On the Multi-modal Vulnerability of Diffusion Models

Dingcheng Yang^{1,*}, Yang Bai^{2,*}, Xiaojun Jia³, Yang Liu³, Xiaochun Cao⁴, Wenjian Yu^{1,†}

¹Dept. Computer Science & Tech., BNRist, Tsinghua University, Beijing, China.

²Independent Researcher.

³Nanyang Technological University.

⁴Sun Yat-sen University, Shenzhen.

ydc19@mails.tsinghua.edu.cn, baiyang0522@gmail.com, jiaxiaojunq@gmail.com,
yangliu@ntu.edu.sg, caoxiaochun@mail.sysu.edu.cn, yu-wj@tsinghua.edu.cn

Abstract—Diffusion models have been widely deployed in various image generation tasks, demonstrating an extraordinary connection between image and text modalities. Although prior studies have explored the vulnerability of diffusion models from the perspectives of text and image modalities separately, the current research landscape has not yet thoroughly investigated the vulnerabilities that arise from the integration of multiple modalities, specifically through the joint analysis of textual and visual features. In this paper, we are the first to visualize both text and image feature space embedded by diffusion models and observe a significant difference. The prompts are embedded chaotically in the text feature space, while in the image feature space they are clustered according to their subjects. These fascinating findings may underscore a potential misalignment in robustness between the two modalities that exists within diffusion models. Based on this observation, we propose MMP-Attack, which leverages multi-modal priors (MMP) to manipulate the generation results of diffusion models by appending a specific suffix to the original prompt. Specifically, our goal is to induce diffusion models to generate a specific object while simultaneously eliminating the original object. Our MMP-Attack shows a notable advantage over existing studies with superior manipulation capability and efficiency. Our code is publicly available at <https://github.com/ydc123/MMP-Attack>.

1. INTRODUCTION

In recent years, diffusion models [1, 2] have revolutionized the field of image generation, achieving state-of-the-art results in both the diversity and quality of generated content. The advancement of vision-language models [3] has further enhanced the capabilities of diffusion models, giving rise to novel applications in text-to-image (T2I) generation [4, 5, 6, 7, 8]. However, existing studies have shown that diffusion models also exhibit vulnerability issues, where appending a specific suffix to the original prompts can manipulate diffusion models to generate completely different image content. ATM [9] and SAGE [10] have respectively investigated white-box attacks for both untargeted and targeted scenarios. Additionally, Adversarial Prompting (AP) [11] explored query-based targeted attack. However, all three methods demand a significant number of image generations, not only making it time-consuming but also unsuitable for commercial models due to their confidentiality or substantial monetary costs. QF-Attack [12] intro-

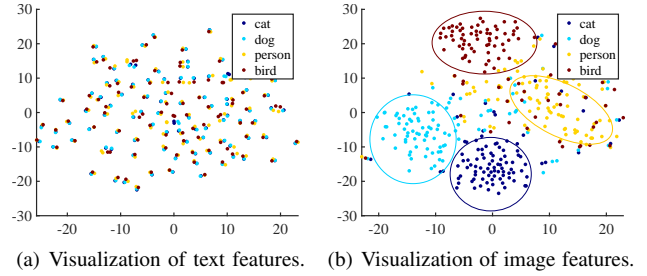


Fig. 1: Visualization of 400 samples in text (left) and image (right) feature space embedded by Stable Diffusion v1.4 (SD v14). Text features are chaotic while image features are clustered.

duces an attack method that does not require image generation, but it is limited to untargeted attack and targeted erasing, namely generating random image content unrelated to the original prompt and omitting a specific category mentioned in the original prompt respectively. MMA-Diffusion [13] optimized adversarial prompts to make T2I models generate Not-Safe-For-Work (NSFW) images. However, it did not consider the issue from a robustness perspective, meaning it did not require modifications on a given original prompt. Consequently, the problem addressed by MMA-Diffusion was relatively easier.

Besides their unsatisfactory performance, existing studies are also limited by their designed algorithms solely on either text or image feature space. In QF-Attack and MMA-Diffusion, the distance from the original prompt and target prompt was calculated in the text feature space. In ATM, SAGE and AP, the objective functions were designed in the image feature space with an auxiliary image classifier, assessing whether the generated images contain objects of predefined categories. The lack of exploration across different modalities inspired us to visualize the text and image feature space within diffusion models simultaneously. A significant difference between the two modalities is thus observed. As shown in Fig. 1, we draw both text and image features of 400 samples embedded by Stable Diffusion v1.4 (SD v14), which are formed with 100 templates and 4 objects. Details of these

*Equal contribution. †Corresponding author.

samples are given in Sec. 3.2. The prompts are embedded chaotically in the text feature space, while in the image feature space they are clustered according to their subjects. This phenomenon can be attributed to the fact that text features distribute their emphasis across a variety of words, consequently placing greater importance on the sentences or templates. In contrast, image features are more concentrated on the specific objects. This difference also highlights certain suboptimal alignments within existing diffusion models, particularly from a robustness standpoint, which we will further analyse in Sec. 3.2.

Based on this observation, we propose an **MMP-Attack** by utilizing **Multi-Modal Priors**. Our approach optimizes a suffix appended to the original prompt, aiming to effectively manipulate T2I diffusion models. Specifically, it facilitates the generation of a desired target object by removing the original object, thus addressing the most challenging scenario. The distance between the optimized prompt and the target category (to add) is minimized in both text and image feature space. The differences between our MMP-Attack and existing works are briefly summarized in Table 1.

TABLE 1: Comparison of existing methods with ours, based on the considered modality, targeted/untargeted setting, and whether image generation is required.

Method	Modality	Goal	Generation-free
ATM	image	Untargeted attack	×
SAGE	image	Targeted attack	×
AP	image	Targeted attack	×
QF-Attack	text	Untargeted attack	✓
MMA-Diffusion	text	NSFW	✓
MMP (Ours)	text+image	Targeted attack	✓

Comprehensive experiments demonstrate the superior universality and transferability of our optimized suffix. Universality indicates that a suffix optimized under a specific prefix can, to some extent, generalize to other prefixes. Transferability indicates that the suffix optimized on an open-source diffusion model can be employed to manipulate a black-box diffusion model, posing a more severe security threat to commercial T2I models, such as DALL-E 3. In this paper, our experimental results show an attack success rate of 50.4% in manipulating Stable Diffusion v2.1 (SD v21) using the suffix generated on SD v14. Moreover, after analyzing the optimized suffix, we observed that MMP-Attack often works in a *cheating* way, which means that it often contains some tokens related to the target object. *It should be noted that simply appending the target object to the original prompt does not work.* Therefore, we also denote the suffix we optimize as a *cheating suffix*.

The major contributions are summarized as follows.

- We conduct a visual analysis of both the text and image feature spaces that are embedded by diffusion models. Our work represents the first instance of observing the notable differences in features across multi-modalities. Such intriguing observations could potentially highlight a misalignment between the two modalities within diffusion models, particularly from the perspective of robustness.

- Based on the observations, we propose **MMP-Attack**, which leverages multi-modal priors (MMP) to targetedly manipulate the generation results of diffusion models. This is achieved by appending a specific suffix after the original prompt, which often contains some tokens related to the target object, hence referred to as a *cheating suffix*.
- Experimental results indicate that our method achieves over 81.8% attack success rates on two open-source T2I models even with only four tokens, showcasing a notable advantage over existing works.

2. RELATED WORK

2.1 Diffusion Models

Diffusion models have achieved remarkable success in the field of image generation through a learnable step-wise denoising process that transforms a simple Gaussian distribution into the data distribution [1]. Some studies have been proposed to accelerating the image generation process [2, 14]. Beyond the field of image synthesis, diffusion models are widely used in diverse fields, including music generation [15], 3D generation [16] and video generation [17]. Notably, by combining with the visual language model CLIP [3], the diffusion model showcases exceptional prowess in text-to-image generation [4, 8].

2.2 Manipulation in T2I Generation

Deep neural networks are known to be vulnerable [18, 19, 20, 21, 22, 23]. Recent studies have shown that the T2I generation process is vulnerable to prompts, indicating that it is possible to manipulate T2I models to generate images unrelated to the given prompt by adding a special suffix to the prompt. ATM [9] and SAGE [10] proposed white-box methods, which assume that the diffusion model is fully known, making it unsuitable for confidential commercial models. AP [11] performed a high-cost query-based method. The practicality of these approaches is limited. QF-Attack [12] assumed that the diffusion model has a white-box CLIP model but an inaccessible and unqueryable generative model. Under this assumption, they proposed a generation-free method against T2I models, which employed a genetic algorithm to manipulate the CLIP model. However, they only considered untargeted attack and targeted erasing. In this paper, we follow the setting outlined in QF-Attack but address a more challenging task: targeted manipulation, specifically by adding target objects while removing original objects in original prompts.

Another line of work in manipulating T2I models involves designing prompts to make the generated content NSFW, such as with MMA-Diffusion [13]. The key difference between MMP-Attack and such approaches is the presence of the original prompt, which makes the problem we are studying significantly more difficult. The algorithm of MMA-Diffusion can be modified to generate *cheating suffixes*, and a comparative experiment with MMP-Attack will also be presented in Sec. 5.2.

3. OBSERVATIONS ON MULTI-MODAL FEATURES WITHIN DIFFUSION MODELS

In this part, we first outline the preliminary of diffusion models. We then define and visualize the text and image feature spaces, thereby highlighting a marked distinction between the multi-modal feature distributions.

3.1 Preliminary: Pipeline of Diffusion Model

Given that the vocabulary of candidate tokens forms a set $\mathbb{V} = \{w_1, w_2, \dots, w_{|\mathbb{V}|}\}$, an input prompt can be expressed as $s \in \mathbb{V}^*$. A well-trained diffusion model consists of two components: a CLIP model and a generative model G . The CLIP model includes an image encoder F^i , which takes an image as input and outputs a d_{emb} -dimensional image embedding vector. It also includes a token embedder E_ψ and a text encoder F^t , which together embed a text prompt into a d_{emb} -dimensional text embedding vector. Here, $\psi \in \mathbb{R}^{|\mathbb{V}| \times d_{\text{token}}}$ serves as an embedding codebook. For the input prompt s , $E_\psi(s)$ is a matrix of shape $|s| \times d_{\text{token}}$, where $E_\psi(s)_i = \psi_{j_i}$ with the condition that $w_{j_i} = s_i$. This token embedding matrix $E_\psi(s)$ is then input into the text encoder F^t and embedded as a d_{emb} -dimensional text embedding vector. During the training stage, an image is transformed to an image embedding vector by the image encoder. Simultaneously, its caption (text data) is transformed to a text embedding vector by the token embedder and the text encoder. The distance between the two vectors is minimized to enable the CLIP model to align the image space and text space. During the T2I generation stage, the input prompt s is first embedded into a text embedding vector v by the token embedder and text encoder. Then, it is input into the subsequent generative model G to sample $x \sim G(v)$, where $G(v)$ is a probability distribution conditioned on v , and x represents a sampled image. Thus, the T2I generation from the input prompt s can be understood as a process of sampling from the probability distribution $x \sim G(F^t(E_\psi(s)))$.

3.2 Multi-modal Features in Diffusion Models

Previous studies have separately investigated the vulnerability of diffusion models from the perspectives of text and image modalities [10, 12]. In contrast to their studies, we investigate the vulnerability of multi-modal features. Given a prompt s , we define its text embedding vector as $F^t(E_\psi(s))$, and its image embedding vector as $F^i(x)$, where $x \sim G(F^t(E_\psi(s)))$. Then, we visualize the text and image feature spaces, showcasing a marked distinction between the multi-modalities.

Chaos Effect of Features in Text Space. We first visualize the text feature space. We instructed ChatGPT to generate 100 prompt templates, and then sequentially filled in ‘cat’, ‘dog’, ‘bird’, and ‘person’ sequentially as subjects to form 400 prompts. Then, we embedded these 400 prompts into text embedding vectors by the SD v14 and visualized them in the text feature space using t-SNE. The visualization results is shown in Fig. 1(a), illustrating that prompts associated with different subjects are mixed together. This is because both the subjects and other tokens are considered important by the text encoder. Thus, in the text feature space, prompts

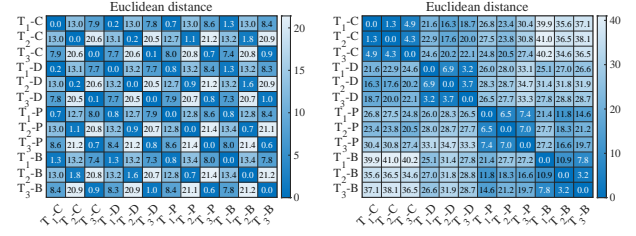


Fig. 2: Euclidean distances between 12 different prompts in the text (left) and image (right) feature spaces. The prompts are generated from 3 different templates: ‘a {noun} is sitting on a bench in a park’, ‘a {noun} is peeking out from behind a curtain’, and ‘a {noun} is standing at the edge of a cliff’, denoted as T_1 , T_2 , and T_3 , respectively. ‘-C’, ‘-D’, ‘-P’, and ‘-B’ represent the {noun} being cat, dog, person, and bird respectively.

with different subjects but originating from the same template can be embedded close together. This implies that even if two prompts are close in the text feature space, they may have different subjects. To illustrate this phenomenon more clearly, we chose 12 prompts originating from 3 templates and calculated their Euclidean distances from each other, as shown in Fig. 2(a).

Clustering Effect of Features in Image Space. Then, we use SD v14 to visualize these 400 prompts on the image feature space, as shown in Fig. 1(b). It can be observed that the embedding vectors of these prompts have remarkably different distributions on the image feature space than on the text feature space, revealing the potential misalignment between text feature space and image feature space for diffusion models. Specifically, the prompts with the same subject are clustered together in the image feature space, while prompts with different subjects are distinguished from each other. This difference arises because the text encoder extracts features of all tokens in the prompts, while an image encoder primarily extracts features of the key object (subject) in the images. Thus, the prompts that are close in the image feature space often share the same subject. This can be evidenced in Fig. 2(b), where the distances of prompt pairs with the same subject are significantly lower (up to 10.9) in the image feature space.

4. METHODOLOGY

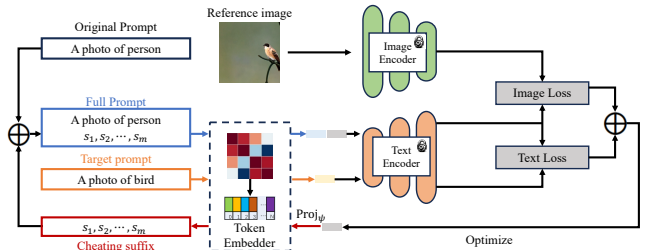


Fig. 3: An illustration of the proposed MMP-Attack flow.

In this part, we propose MMP-Attack, which leverages multi-modal priors to targeted attack the T2I generation. We begin by formulating the targeted attack problem for T2I models. Then, motivated by the misalignment phenomenon observed in Sec. 3, we propose an optimization objective that simultaneously considers both the image and text modalities. Finally, we present the corresponding optimization approach. An illustration of our MMP-Attack is shown in Fig. 3.

4.1 Problem Formulation

Let $s_o \in \mathbb{V}^n$ be the original prompt containing n tokens, and m be the number of tokens in the cheating suffix. The cheating suffix to be optimized can be represented as $s_a \in \mathbb{V}^m$, which will be concatenated with s_o to get the full prompt $s_o \oplus s_a \in \mathbb{V}^{n+m}$, where the operator \oplus denotes concatenation operator.

For conducting targeted attack, we assume that there is a target category $t \in \mathbb{V}$ (e.g., dog, bird). This target category is irrelevant to the original prompt s_o . We need to search for a cheating suffix that, when concatenated with the original prompt s_o , guides the T2I diffusion model to generate an image containing the target category but is unrelated to s_o . The optimization objective is as follows:

$$\operatorname{argmax}_{s_a} \mathbb{E}_{x \sim G(F^t(E_\psi(s_o \oplus s_a)))} \mathcal{A}(x, t, s_o), \quad (1)$$

where x represents a randomly generated image based on the full prompt $s_o \oplus s_a$. The $\mathcal{A}(x, t, s_o)$ is an evaluation metric to assess the manipulation performance. Following the assumptions of relevant work [12], during the optimization process, we have access only to the CLIP model and are blind to the generative model G , which can only be used for evaluating the manipulation performance of the cheating suffix.

To ensure the naturalness of the cheating suffix, we refined the vocabulary \mathbb{V} to include only English words that end with the ' $\langle /w \rangle$ ' symbol, indicating a white-space. This step was necessary because the CLIP vocabulary includes tokens representing prefixes that do not end with ' $\langle /w \rangle$ ', and the concatenation of such tokens could result in the optimized cheating suffix containing non-existent words, thereby reducing the naturalness of the prompt. Furthermore, we additionally filtered out the top-20 synonyms of the target category from the vocabulary, to simulate real-world systems that block sensitive words. Specifically, the embedding codebook ψ was employed to define the similarity between two tokens w_i, w_j as $\cos(\psi_i, \psi_j)$, where $\cos(a, b) = \frac{a^T b}{\|a\| \|b\|}$ represents the cosine similarity between two vectors.

4.2 Optimization Objective

Directly solving (1) is infeasible, because it involves a generative model G that is unknown in our assumption. An alternative approach is to first construct a target vector v_t that provides a favorable solution to the following optimization objective:

$$\operatorname{argmax}_{v_t} \mathbb{E}_{x \sim G(v_t)} \mathcal{A}(x, t, s_o). \quad (2)$$

Assuming such a v_t exists, we can achieve a favorable solution to (1) by maximizing the similarity between the text embedding vectors of $s_o \oplus s_a$ and target vector v_t . Consequently, the optimization objective (1) is transformed into a simplified problem involving only F^t and E_ψ :

$$\operatorname{argmax}_{s_a} \cos(F^t(E_\psi(s_o \oplus s_a)), v_t). \quad (3)$$

Although G is unknown, constructing a favorable solution for problem (2) is not difficult, since we can use some heuristics solutions. For example, the images generated by a manually crafted prompt $s' = \text{'a photo of } t \text{'}$ will undoubtedly satisfy the requirements of our targeted attack. Thus, we can utilize its text embedding vector $v_t^{\text{text}} = F^t(E_\psi(s'))$ as a target vector to guide the optimization of cheating suffix.

However, as demonstrated in Sec. 3, the embedding vectors of prompts in the text feature space and the image feature space are misaligned. This implies that even though prompts have relatively close distances in the text feature space, the resulting images could be far apart in the image feature space, indicating differences in key objects present in the images. Thus, we integrate image modal information with text modal to guide the optimization process. Since the generative model G is unknown, we cannot compute loss terms for generated images, as done in prior work [10, 11]. Instead, we propose a target vector based on image modality. This approach also avoids the costly image generation required in prior work that utilized the image modality. Specifically, given a reference image x_t containing the target category, we calculate its image embedding vector $v_t^{\text{image}} = F^i(x_t)$, where F^i is the image encoder of the CLIP model. The CLIP model possesses the characteristic that image-text pairs with higher correlation exhibit larger cosine similarities in their embedding vectors. Therefore, v_t^{image} is also a favorable solution for (2). Finally, we concurrently optimize in both the image and text modalities, where the multi-modal loss is designed as maximizing the similarity between the text embedding vector of $s_o \oplus s_a$ and the two target vectors, as shown in Fig. 3. The optimization objective is as follows:

$$\begin{aligned} \operatorname{argmax}_{s_a} \cos(v, v_t^{\text{image}}) + \lambda \cos(v, v_t^{\text{text}}), \\ \text{s.t. } v = F^t(E_\psi(s_o \oplus s_a)), \end{aligned} \quad (4)$$

where λ is a weighting factor to balance the loss terms between the image and text modalities.

4.3 Optimization Approach

The remaining challenge lies in solving (4). As the optimization variables are defined in a discrete space, it presents a combinatorial optimization problem that is non-differentiable and often NP-hard. To address this issue, a commonly used technique is Straight-Through Estimation (STE) technique [24], which introduces a differentiable function $\text{sg}(\cdot)$ that is defined as the identity function during forward propagation and has zero partial derivatives. It has been previously applied in other discrete optimization domains, including neural network quantization [25, 26], and training discrete generative models such as VQ-VAE [27] and VQ-GAN [28]. Inspired

Algorithm 1 MMP-Attack

Input: token embedder E_ψ , dimension of the token embedding vector d_{token} , text encoder F^t , image encoder F^i , learning rate η , number of iterations N , original prompt s_o , number of tokens in cheating suffix m , target category $t \in \mathbb{V}$, weighting factor λ , a reference image x_t containing the target category t and unrelated to original prompt s_o .
Output: Cheating suffix s_a .

```
1:  $v_t^{\text{image}} \leftarrow F^i(x_t)$ .
2:  $s' \leftarrow \text{'a photo of } t'$ .
3:  $v_t^{\text{text}} = F^t(E_\psi(s'))$ 
4: Initialize  $Z \in \mathbb{R}^{m \times d_{\text{token}}}$ .
5:  $\text{bestloss} \leftarrow \infty, \text{best}Z \leftarrow Z$ 
6: for  $i \leftarrow 1$  to  $N$  do
7:    $v \leftarrow F^t(E_\psi(s_o) \oplus \text{Proj}_\psi(Z))$ .
8:    $\mathcal{L} = -\cos(v, v_t^{\text{image}}) - \lambda \cos(v, v_t^{\text{text}})$ .
9:   if  $\text{bestloss} > \mathcal{L}$  then
10:     $\text{bestloss} \leftarrow \mathcal{L}, \text{best}Z \leftarrow Z$ .
11:   end if
12:    $Z \leftarrow Z - \eta \nabla_Z \mathcal{L}$ .
13: end for
14:  $s_a \leftarrow E_\psi^{-1}(\text{Proj}_\psi(\text{best}Z))$ .
```

by these works, we leverage the $\text{sg}(\cdot)$ function to solve (4). Specifically, we optimize the token embedding matrix $Z \in \mathbb{R}^{m \times d_{\text{token}}}$ of the cheating suffix, and define a differentiable function $\text{Proj}_\psi : \mathbb{R}^{m \times d_{\text{token}}} \rightarrow \mathbb{R}^{m \times d_{\text{token}}}$, where $\text{Proj}_\psi(Z)_i = Z_i + \text{sg}(\psi_j - Z_i)$ such that $j = \text{argmin}_{j'} \|\psi_{j'} - Z_i\|_2^2$. Notice that each row in matrix $\text{Proj}_\psi(Z)$ corresponds to an entry in the codebook ψ , therefore we can decode the cheating suffix $s_a = E_\psi^{-1}(\text{Proj}_\psi(Z))$. Moreover, due to the property $E_\psi(s_o \oplus s_a) = E_\psi(s_o) \oplus E_\psi(s_a)$, (4) can be reformulated into the following optimization problem:

$$\begin{aligned} & \text{argmax}_Z \cos(v, v_t^{\text{image}}) + \lambda \cos(v, v_t^{\text{text}}) \\ \text{s.t. } & v = F^t(E_\psi(s_o \oplus s_a)) \\ & = F^t(E_\psi(s_o \oplus E_\psi^{-1}(\text{Proj}_\psi(Z)))) \\ & = F^t(E_\psi(s_o) \oplus \text{Proj}_\psi(Z)). \end{aligned} \quad (5)$$

Because the Proj function is differentiable, (5) can be solved using a gradient-based optimizer, providing better performance compared to prior work [12] that employs a zero-order optimizer. Our optimization approach is summarized in Algorithm 1. The target conditional vectors are first calculated in Step 1-3. Then, the optimization variable Z is initialized and optimized by a gradient descent algorithm (Step 4-13). Finally, the cheating suffix is decoded based on the optimized Z (Step 14).

A good initialization (Step 4) often helps reduce the complexity of the optimization problem, leading to better solutions [29]. To solve (5), we consider three initialization methods:

- 1) **EOS:** Initialize all Z_i as the token embedding for $[\text{eos}]$, where $[\text{eos}]$ is a special token in CLIP

vocabulary representing the end of string.

- 2) **Random:** Randomly sample m tokens from the filtered vocabulary and use their embeddings as the initial values for Z .
- 3) **Synonym:** Select the token with the highest cosine similarity to the target category t in the filtered vocabulary, and use its token embedding as the initial values for all Z_i .

The synonym initialization is used by default, and an ablation study on the initialization method is presented in Sec. 5.4.

5. EXPERIMENTS

5.1 Settings

Dataset. Five object categories are selected from the Microsoft COCO dataset [30], namely car, dog, person, bird, and knife. They are considered as both the original and target categories, forming a total of $5 \times 4 = 20$ distinct category pairs. For each category pair, a cheating suffix is generated. Each cheating suffix is then used to generate 100 images to evaluate the manipulation performance metrics. The final performance metrics are obtained by averaging across all categories, which means that for a given method, its performance metrics are calculated over $5 \times 4 \times 100 = 2000$ images.

Models. Following the setting in relevant work [12], we initially employ Stable Diffusion v1.4 (SD v14)¹ as the diffusion model for image generation and performance evaluation. This model utilizes a pretrained CLIP model, which is trained on a dataset containing text-image pairs [31]. Furthermore, we also consider an additional model, Stable Diffusion v2.1 (SD v21)², which has a distinct CLIP model compared to SD v14. During image generation, the resolution is set to 512×512 , the number of inference step is set to 50, and the classifier-free guidance scale is set to 7.5. Finally, we also consider commercial T2I services, i.e., DALL-E 3 [32] and Imagine Art.

Evaluation Metrics. Given a generated image, the following metrics are considered to evaluate the manipulation performance: 1) **CLIP score:** We use the CLIP [3] model to calculate the embedding vectors for the generated image and the prompt ('a photo of t '), subsequently determining their matching score based on cosine similarity. 2) **BLIP score:** BLIP [33] is a better visual-language model. We use it to compute the image-text matching score. 3) **Original Category Non-Detection Rate (OCNDR):** A binary metric where we employ an object detection model to examine if the generated image fails to detect objects of the original category, indicating an untargeted attack. 4) **Target Category Detection Rate (TCDR):** Similar to OCNDR, it is a binary metric where we use an object detection model to check if the generated image contains objects of the target category. 5) **BOTH:** A binary metric where the value is 1 if and only if

¹<https://huggingface.co/CompVis/stable-diffusion-v1-4>

²<https://huggingface.co/stabilityai/stable-diffusion-2-1>

both OCNDS and TCDR are 1. A pretrained faster R-CNN model [34] with a ResNet-50-FPN backbone [35] is utilized as the object detection model to evaluate OCNDR, TCDR and BOTH, which is publicly available at torchvision.

We consider two experimental settings: 1) **Grey-box**: In this setting, the generative model G is unknown and we cannot query it. However, we assume that the CLIP model, composed of E_ψ , F^t , and F^i , is known. This assumption arises from the considerable computational cost of training a CLIP model. Consequently, existing diffusion models, such as stable diffusion [4], often leverage an open-source CLIP model. 2) **Black-box**: Additionally, we considered a more challenging setting where the CLIP model is also unknown. We adopt a transfer-based strategy, where a white-box CLIP model is chosen as surrogate. Subsequently, we leverage this surrogate model to search a cheating suffix. Finally, the searched cheating suffix is employed to manipulate black-box T2I models. The grey-box setting is adopted to generate cheating suffix directly, while the black-box setting is adopted mainly to evaluate the transferability. **Unless otherwise specified, experiments are conducted within grey-box setting.**

5.2 Main Results

We use MMP-Attack to optimize cheating suffixes, each comprising four tokens ($m = 4$). For comparative purposes, we consider four baseline methods: 1) **No attack**, meaning no cheating suffix is added; 2) **Random**, where four tokens are randomly chosen to form the cheating suffix; 3) **QF-Attack** [12], a method that proposed a genetic algorithm for untargeted attack, aiming to maximize the distance in text feature space from the original prompt; 4) **MMA-Diffusion** [13]: a method that used greedy coordinate gradient [36] to make diffusion models to generate NSFW images. The implementation details and modifications for targeted attacks of these attack methods are presented in Appendix A, while ablation studies provided in Sec. 5.4.

Attacking results of MMP-Attack and comparative experiments with baselines are listed in Table 2. From the table, we can see that all baseline methods exhibit relatively weak performance. This highlights the difficulty of the targeted attack setting. Then, Table 2 also demonstrates a substantial superiority of MMP-Attack over the baselines. Specifically, for the BOTH score, MMP-Attack surpasses the strongest baseline MMA-Diffusion by 38.6% and 56.5% on SD v14 and SD v21, respectively. This metric offers an intuitive reflection of attack success rates, requiring the generated images not only exclude the original category but also contain the target category. As a byproduct, MMP-Attack can also manipulate T2I models to generate NSFW images, as demonstrated in Appendix B.

Then, we present some results in Fig. 4, showcasing cheating suffixes discovered by MMP-Attack alongside the generated images. More results are presented in Appendix C. By analyzing these suffixes, we observe that MMP-Attack automatically identifies specific tokens to achieve the manipulation goal. The identified tokens could be relevant words associated with the target object that were not filtered out during the

TABLE 2: Results of different methods. The metrics are defined in Sec. 5.1. **Best results are boldfaced.**

Model	Method	CLIP	BLIP	OCNDR	TCDR	BOTH
SD v14	No attack	0.200	0.014	1.6%	0.9%	0.0%
	Random	0.202	0.013	2.4%	1.3%	0.1%
	QF-Attack	0.223	0.066	19.7%	27.4%	14.2%
	MMA-Diffusion	0.244	0.229	49.9%	51.0%	43.2%
	MMP-Attack (Ours)	0.265	0.414	92.0%	87.2%	81.8%
SD v21	No attack	0.204	0.019	5.0%	1.6%	0.1%
	Random	0.203	0.015	5.4%	1.9%	0.6%
	QF-Attack	0.206	0.021	18.7%	11.1%	5.5%
	MMA-Diffusion	0.239	0.205	47.2%	34.6%	29.9%
	MMP-Attack (Ours)	0.270	0.429	95.2%	91.0%	86.4%



Fig. 4: Examples of optimized cheating suffixes (marked in red) and their corresponding generated images.

preprocessing stage. For example, when the categories are `car` and `person`, our MMP-Attack can automatically identify relevant tokens such as `buick` and `andre washington`, respectively. The resulting cheating suffixes not only guide the T2I model to generate the desired objects but also lead it to ignore the original prompt. Moreover, in the task of targeting `car` to `bird`, all four tokens are unrelated to birds. Thus, when using `rwby`, `migration`, `reed` and `mone` as cheating suffixes separately, the T2I model generates images of cars (see Fig. 5). However, when using all four tokens simultaneously, it generates images of birds.

5.3 Universality and Transferability

We have shown that, the optimized cheating suffix s_a can overwrite the content of original prompt s_o and generates an image of the target category t . By observing Fig. 4, it can be noticed that the two cheating suffixes discovered for the target category `bird` contain similar tokens, namely both include `rwby`, and one includes `migrant` while the other includes `migration`. This inspires us to explore whether the cheating suffix optimized for one category may be effective for other category pairs within the same target category, referred to as universality. We first attempt to append the cheating suffix ‘`wild blers rwby migrant`’ to `car`, `dog`, and `knife`, and show the generated results in Fig. 6. Surprisingly, even though the original categories are not considered during the optimization process, we find out that the targeted attack still succeeded. Then, we systematically evaluate the universality of 20 cheating suffixes optimized for SD v14. We evaluate their effectiveness in targeted attack on the other three categories and present the BOTH score in Table 3. All cases exhibit a certain degree of universality, with the highest reaching up to 99%.

Next, we will demonstrate that our cheating suffixes exhibit transferability, meaning that cheating suffixes crafted to

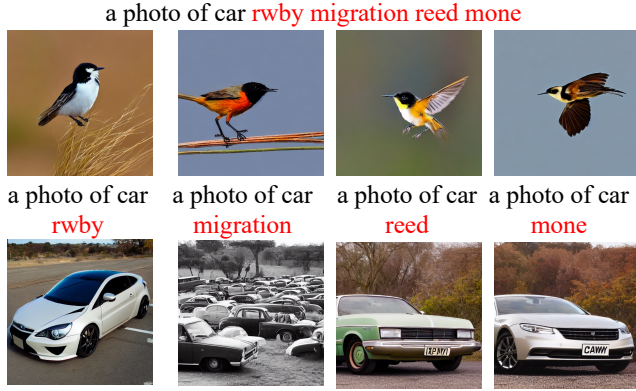


Fig. 5: The images generated by SD v14 using different cheating suffixes (marked in red). The top four images are generated using the cheating suffix we optimized. The bottom four images are respectively generated using each of the four individual tokens as the cheating suffix.

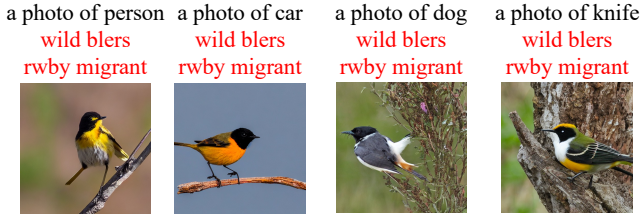


Fig. 6: Examples of universality on SD v14. The cheating suffix marked in red is optimized with the original category person and the target category bird. It works well on different original prompts.

manipulate one diffusion model can also be effective against another diffusion model. This phenomenon has given rise to transfer-based **black-box** manipulation, as discussed in Sec. 5.1. Below, we use cheating suffixes generated from SD v14 to manipulate SD v21, and vice versa, use cheating suffixes generated from SD v21 to manipulate SD v14. The experimental results are listed in Table 4, where BOTH scores of 66.8% and 50.4% are achieved for SD v14 and SD v21, respectively. By comparing with Table 2, it can be observed that the performance degrades in the black-box manipulation scenario but still outperforms all the baselines. Some transfer-based results are presented in in Fig. 7. Additionally, we present some black-box manipulation results conducted on commercial T2I online services, including DALL-E 3 and Imagine Art, in Appendix D.

5.4 Ablation Study

In this part, we delve into the crucial aspect of ablation studies, focusing on two key elements: the initialization method and multi-modal objective functions.

Initialization Methods. We investigate the impact of different initialization methods on manipulation performance. We conduct experiments on SD v14 and present the experimental results in Table 5, which shows that the EOS initialization performs the worst. This is because the `[eos]` token is not



Fig. 7: Examples of **black-box** transferability. ‘SD v14 → SD v21’ indicates manipulating SD v21 using the cheating suffix obtained for manipulating SD v14, and vice versa for ‘SD v21 → SD v14’.

TABLE 3: Universal attack success rates of MMP-Attack against SD v14. The value in each cell is obtained by averaging BOTH score across the other three categories, excluding the original category (corresponding to the row) and the target category (corresponding to the column), over a total of 3×100 generated images.

	car	person	bird	dog	knife
car	-	66.0%	54.7%	52.3%	88.7%
person	58.3%	-	93.3%	41.3%	89.7%
bird	66.0%	76.7%	-	62.0%	80.7%
dog	39.7%	99.0%	69.3%	-	68.0%
knife	34.0%	63.0%	81.3%	86.3%	-

included in the filtered vocabulary, causing the Proj function to project it onto a distant word at the beginning. This phenomenon will impair the STE technique. In contrast, the ‘Random’ and ‘Synonym’ initialization allow the projection function to degenerate into an identity function at the initial value, enabling STE to provide a sufficiently accurate gradient at the beginning of optimization. Furthermore, the ‘Synonym’ initialization offers a more intuitively better initial solution compared to ‘Random’. Thus, it leads to better results and serves as our default choice.

Multi-modal Objectives. We further investigate the impact of the weighting factor λ on the manipulation performance, where λ represent the importance of the text modal loss term. We enumerate different values of λ from $\{0, 0.001, 0.01, 0.1, 0.25, 0.5, 0.75, 1\}$ and plotted the manipulation results on SD v14 in Figure 8. When $\lambda = 0$, it implies a method using only the **Image-Modal Prior** (we call it **IMP-Attack**), corresponding to the dashed line. Figure 8 shows that when λ is small, the manipulation performance is similar to IMP-Attack, and it increases as λ increases. However, when λ exceeds 0.1, the manipulation performance starts to decrease rapidly. This phenomenon indicates that the image modality plays a more prominent role in MMP-Attack. Furthermore, the alignment between these two modalities is not consistently optimal due to their inherent conflicting performance characteristics during attack. Therefore, incorporating both text and image features into an attack can be advantageous.

6. CONCLUSIONS

In this paper, we analyze the vulnerability of manipulating diffusion models from a novel perspective of multi-modality.

TABLE 4: **Black-box** targeted attack results. ‘SD v14 \rightarrow SD v21’ indicates manipulating SD v21 using the cheating suffix obtained for manipulating SD v14, and vice versa for ‘SD v21 \rightarrow SD v14’. The metrics are defined in Sec. 5.1.

Setting	CLIP	BLIP	OCNDR	TCDR	BOTH
SD v14 \rightarrow SD v21	0.243	0.231	72.3%	62.2%	50.4%
SD v21 \rightarrow SD v14	0.247	0.235	71.3%	74.9%	66.8%

TABLE 5: Results of different initialization methods on SD v14. The metrics are defined in Section 5.1. **Best results are bolded.**

Initialization	CLIP	BLIP	OCNDR	TCDR	BOTH
EOS	0.262	0.390	82.2%	78.3%	72.3%
Random	0.263	0.400	84.1%	82.0%	74.4%
Synonym	0.265	0.414	92.0%	87.2%	81.8%

We are the first to observe a significant misalignment between the two modalities, particularly from the perspective of robustness. We further find that the text encoder spreads its attention across different words within a sentence and is therefore less sensitive to the main object, but is mainly affected by the sentence template. In contrast, image features are clearly clustered with their objects, showing a clear focus on words related to the objects. Therefore, incorporating both text and image features into an attack can be advantageous. Motivated by this intriguing observation, we propose **MMP-Attack**, which leverages multi-modal priors (MMP) to targeted manipulate the generation results of diffusion models. The *cheating suffix* generated by MMP-Attack exhibits extraordinary performance, demonstrating not only high attack success rates but also superior universality and transferability. Our work contributes to a deeper understanding of T2I generation and establishes a novel paradigm for adversarial studies in AI-generated content (AIGC).

REFERENCES

- [1] J. Ho, A. Jain, and P. Abbeel, “Denoising diffusion probabilistic models,” *Advances in neural information processing systems*, vol. 33, pp. 6840–6851, 2020.
- [2] J. Song, C. Meng, and S. Ermon, “Denoising diffusion implicit models,” in *International Conference on Learning Representations*, 2020.
- [3] A. Radford, J. W. Kim, C. Hallacy, A. Ramesh, G. Goh, S. Agarwal, G. Sastry, A. Askell, P. Mishkin, J. Clark *et al.*, “Learning transferable visual models from natural language supervision,” in *International conference on machine learning*. PMLR, 2021, pp. 8748–8763.
- [4] R. Rombach, A. Blattmann, D. Lorenz, P. Esser, and B. Ommer, “High-resolution image synthesis with latent diffusion models,” in *Proceedings of the IEEE/CVF conference on computer vision and pattern recognition*, 2022, pp. 10 684–10 695.
- [5] A. Ramesh, P. Dhariwal, A. Nichol, C. Chu, and M. Chen, “Hierarchical text-conditional image generation with clip latents,” *arXiv preprint arXiv:2204.06125*, vol. 1, no. 2, p. 3, 2022.

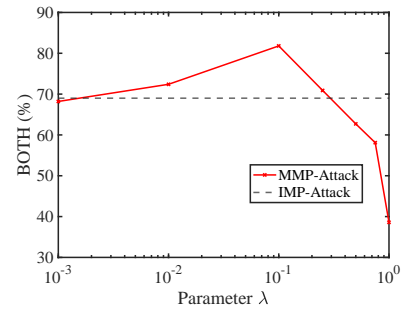


Fig. 8: The BOTH scores versus λ . The dashed line indicates an IMP-Attack, using only the image modal prior($\lambda = 0$).

- [6] A. Q. Nichol, P. Dhariwal, A. Ramesh, P. Shyam, P. Mishkin, B. McGrew, I. Sutskever, and M. Chen, “Glide: Towards photorealistic image generation and editing with text-guided diffusion models,” in *International Conference on Machine Learning*. PMLR, 2022, pp. 16 784–16 804.
- [7] C. Saharia, W. Chan, S. Saxena, L. Li, J. Whang, E. L. Denton, K. Ghasemipour, R. Gontijo Lopes, B. Karagol Ayan, T. Salimans *et al.*, “Photorealistic text-to-image diffusion models with deep language understanding,” *Advances in Neural Information Processing Systems*, vol. 35, pp. 36 479–36 494, 2022.
- [8] R. Gal, Y. Alaluf, Y. Atzmon, O. Patashnik, A. H. Bermano, G. Chechik, and D. Cohen-or, “An image is worth one word: Personalizing text-to-image generation using textual inversion,” in *The Eleventh International Conference on Learning Representations*, 2023.
- [9] C. Du, Y. Li, Z. Qiu, and C. Xu, “Stable diffusion is unstable,” *Advances in Neural Information Processing Systems*, vol. 36, 2024.
- [10] Q. Liu, A. Kortylewski, Y. Bai, S. Bai, and A. Yuille, “Discovering failure modes of text-guided diffusion models via adversarial search,” in *The Twelfth International Conference on Learning Representations*, 2024.
- [11] N. Maus, P. Chao, E. Wong, and J. R. Gardner, “Black box adversarial prompting for foundation models,” in *The Second Workshop on New Frontiers in Adversarial Machine Learning*, 2023.
- [12] H. Zhuang, Y. Zhang, and S. Liu, “A pilot study of query-free adversarial attack against stable diffusion,” in *Proceedings of the IEEE/CVF Conference on Computer Vision and Pattern Recognition*, 2023, pp. 2384–2391.
- [13] Y. Yang, R. Gao, X. Wang, T.-Y. Ho, N. Xu, and Q. Xu, “Mma-diffusion: Multimodal attack on diffusion models,” in *Proceedings of the IEEE/CVF Conference on Computer Vision and Pattern Recognition*, 2024, pp. 7737–7746.
- [14] C. Lu, Y. Zhou, F. Bao, J. Chen, C. Li, and J. Zhu, “Dpm-solver: A fast ode solver for diffusion probabilistic model sampling in around 10 steps,” *Advances in Neural Information Processing Systems*, vol. 35, pp. 5775–5787, 2022.

- [15] Q. Huang, D. S. Park, T. Wang, T. I. Denk, A. Ly, N. Chen, Z. Zhang, Z. Zhang, J. Yu, C. Frank *et al.*, “Noise2music: Text-conditioned music generation with diffusion models,” *arXiv preprint arXiv:2302.03917*, 2023.
- [16] Z. Wang, C. Lu, Y. Wang, F. Bao, C. Li, H. Su, and J. Zhu, “Prolificdreamer: High-fidelity and diverse text-to-3d generation with variational score distillation,” in *Advances in Neural Information Processing Systems (NeurIPS)*, 2023.
- [17] A. Blattmann, T. Dockhorn, S. Kulal, D. Mendelevitch, M. Kilian, D. Lorenz, Y. Levi, Z. English, V. Voleti, A. Letts *et al.*, “Stable video diffusion: Scaling latent video diffusion models to large datasets,” *arXiv preprint arXiv:2311.15127*, 2023.
- [18] C. Szegedy, W. Zaremba, I. Sutskever, J. Bruna, D. Erhan, I. Goodfellow, and R. Fergus, “Intriguing properties of neural networks,” in *ICLR*, 2014.
- [19] Z. Zhao, Z. Liu, and M. Larson, “On success and simplicity: A second look at transferable targeted attacks,” *Advances in Neural Information Processing Systems*, vol. 34, pp. 6115–6128, 2021.
- [20] D. Yang, Z. Xiao, and W. Yu, “Boosting the adversarial transferability of surrogate models with dark knowledge,” in *2023 IEEE 35th International Conference on Tools with Artificial Intelligence (ICTAI)*. IEEE, 2023, pp. 627–635.
- [21] D. Yang, W. Yu, Z. Xiao, and J. Luo, “Generating adversarial examples with better transferability via masking unimportant parameters of surrogate model,” in *2023 International Joint Conference on Neural Networks (IJCNN)*, 2023, pp. 01–08.
- [22] Y. Bai, Y. Zeng, Y. Jiang, Y. Wang, S.-T. Xia, and W. Guo, “Improving query efficiency of black-box adversarial attack,” in *Computer Vision—ECCV 2020: 16th European Conference, Glasgow, UK, August 23–28, 2020, Proceedings, Part XXV 16*. Springer, 2020, pp. 101–116.
- [23] Y. Bai, Y. Wang, Y. Zeng, Y. Jiang, and S.-T. Xia, “Query efficient black-box adversarial attack on deep neural networks,” *Pattern Recognition*, vol. 133, p. 109037, 2023.
- [24] Y. Bengio, N. Léonard, and A. Courville, “Estimating or propagating gradients through stochastic neurons for conditional computation,” *arXiv preprint arXiv:1308.3432*, 2013.
- [25] D. Yang, W. Yu, H. Mu, and G. Yao, “Dynamic programming assisted quantization approaches for compressing normal and robust dnn models,” in *Proceedings of the 26th Asia and South Pacific Design Automation Conference*, 2021, pp. 351–357.
- [26] D. Yang, W. Yu, X. Ding, A. Zhou, and X. Wang, “Dp-nets: Dynamic programming assisted quantization schemes for dnn compression and acceleration,” *Integration*, vol. 82, pp. 147–154, 2022.
- [27] A. Van Den Oord, O. Vinyals *et al.*, “Neural discrete representation learning,” *Advances in neural information processing systems*, vol. 30, 2017.
- [28] P. Esser, R. Rombach, and B. Ommer, “Taming transformers for high-resolution image synthesis,” in *Proceedings of the IEEE/CVF conference on computer vision and pattern recognition*, 2021, pp. 12 873–12 883.
- [29] Y. Tashiro, Y. Song, and S. Ermon, “Diversity can be transferred: Output diversification for white-and black-box attacks,” *Advances in neural information processing systems*, vol. 33, pp. 4536–4548, 2020.
- [30] T.-Y. Lin, M. Maire, S. Belongie, J. Hays, P. Perona, D. Ramanan, P. Dollár, and C. L. Zitnick, “Microsoft coco: Common objects in context,” in *Computer Vision—ECCV 2014: 13th European Conference, Zurich, Switzerland, September 6–12, 2014, Proceedings, Part V 13*. Springer, 2014, pp. 740–755.
- [31] B. Thomee, D. A. Shamma, G. Friedland, B. Elizalde, K. Ni, D. Poland, D. Borth, and L.-J. Li, “Yfcc100m: The new data in multimedia research,” *Communications of the ACM*, vol. 59, no. 2, pp. 64–73, 2016.
- [32] J. Betker, G. Goh, L. Jing, T. Brooks, J. Wang, L. Li, L. Ouyang, J. Zhuang, J. Lee, Y. Guo *et al.*, “Improving image generation with better captions,” *Computer Science*. <https://cdn.openai.com/papers/dall-e-3.pdf>, 2023.
- [33] J. Li, D. Li, C. Xiong, and S. Hoi, “Blip: Bootstrapping language-image pre-training for unified vision-language understanding and generation,” in *International Conference on Machine Learning*. PMLR, 2022, pp. 12 888–12 900.
- [34] S. Ren, K. He, R. Girshick, and J. Sun, “Faster r-cnn: Towards real-time object detection with region proposal networks,” *Advances in neural information processing systems*, vol. 28, 2015.
- [35] T.-Y. Lin, P. Dollár, R. Girshick, K. He, B. Hariharan, and S. Belongie, “Feature pyramid networks for object detection,” in *Proceedings of the IEEE conference on computer vision and pattern recognition*, 2017, pp. 2117–2125.
- [36] A. Zou, Z. Wang, J. Z. Kolter, and M. Fredrikson, “Universal and transferable adversarial attacks on aligned language models,” *arXiv preprint arXiv:2307.15043*, 2023.

APPENDIX A IMPLEMENTATION DETAILS

MMP-Attack: The Adam optimizer is employed for searching cheating suffix. The learning rate is set to 0.001 and the number of optimization iterations is set to 10000. For a single category pair, MMP-Attack takes approximately 6 minutes to run on a single Nvidia RTX 4090 GPU. The synonym initialization method is employed by default, with λ set to 0.1 as the default weighting factor. The reference images used to calculate the loss term for image modality are presented in Figure 9. Table 6 lists the words that are filtered out for each target category, as discussed in Section 4.1. The cosine similarity is calculated using a token embedder from Stable Diffusion v1.4. These filtered words are mostly synonyms of the target category, or otherwise words with strong relevance. This filtering process mimics the use of a sensitive word filtering system commonly employed in real-world application.

QF-Attack: QF-Attack [12] is a method that proposed a genetic algorithm for untargeted attack, aiming to maximize the distance in text feature space from the original prompt. It can be directly extended as a baseline for targeted attack by minimizing the distance in text feature space from the target prompt $s' = \text{'a photo of } t'$. In [12], the number of generation step is set to 50, the number of candidates per step is set to 20, and the length of the cheating suffix is only set to 5 characters. Since this paper focuses on the more challenging targeted attack task, we set the number of generation step to 500. This implies a total of $500 \times 20 = 10000$ forward propagations, which also ensures fairness in computational cost comparison with MMP-Attack. Considering that the cheating suffix in [12] has a length of only 5 characters, which is usually shorter than the length of four tokens we used. To be fair, we employ the genetic algorithm to search for cheating suffix of length 32. This length exceeds the average character length of cheating suffixes searched by MMP-Attack.

MMA-Diffusion: MMA-Diffusion [13] utilizes the greedy coordinate gradient (GCG) method [36] to optimize the loss function in the textual feature space, enabling T2I models to generate not-safe-for-work (NSFW) images. This approach can be adapted for targeted attacks by employing GCG to minimize the distance in the textual feature space between the full prompt $s_o \oplus s_a$ and the target prompt $s' = \text{'a photo of } t'$. We conduct a total of 1000 optimization steps, which generally require around 12 minutes (taking about twice as long as our MMP-Attack).

APPENDIX B NOT-SAFE-FOR-WORK ATTACK RESULTS

MMP-Attack can also be applied in the context of MMA-Diffusion to construct prompts that induce T2I models to generate not-safe-for-work (NSFW) images. We utilized MMP-Attack to create prompts capable of producing NSFW images, using the same blacklisted words as provided by MMA-Diffusion and an empty original prompt. The results are illustrated in Fig. 10. In comparison to Fig. 1 in the MMA-

TABLE 6: List of filtered words. The first row represents the target category, followed by the next 20 rows representing the corresponding filtered words.

car	dog	person	bird	knife
car	dog	person	bird	knife
cars	dogs	people	birds	knives
vehicle	cat	persons	birdie	fork
vehicles	dawg	woman	birdies	sword
dog	doggy	ppl	phone	blade
bus	puppy	guy	fish	wrench
boat	doggy	peoples	cat	gun
automobile	doggo	someone	bee	tool
train	doggie	adult	eagle	guns
van	cats	individual	flight	snakes
bike	horse	thing	birding	inmate
coach	animal	player	horse	weapons
er	pooch	man	birdman	pistol
sedan	car	member	crow	stabbing
i	dawgs	girl	dot	chair
plane	pup	personal	wildlife	spoon
cat	dad	personality	birdwatching	goalie
phone	adog	somebody	knowledge	bike
road	pet	members	plant	stab
suv	hotdog	child	lizard	skateboard

diffusion’s paper [13], it is evident that the prompt we optimized is shorter and less likely to be filtered out.

APPENDIX C DISPLAY OF ALL SEARCHED CHEATING SUFFIXES

We present all the discovered cheating suffixes on SD v14 and SD v21 in Table 7.

APPENDIX D BLACK-BOX TARGETED ATTACK RESULTS

Additionally, we conducted experiments of black-box targeted attacks on a commercial T2I online service, Imagine Art. Some of the results are shown in Figure 11.

Moreover, we also validated the transferability on the commercial model DALL-E 3, which is a popular T2I online service that can be accessed through ChatGPT 4³. Differing from other T2I models, DALL-E 3 automatically refines input prompts to be more user-friendly, mitigating the need for overly complicated prompt engineering. This step increases the difficulty of our transfer-based attacks. Two examples of successful black-box targeted attacks on DALL-E 3 are depicted in Figure 12.

³<https://chat.openai.com/g/g-2fkFE8rbu-dall-e>



Fig. 9: Reference images.

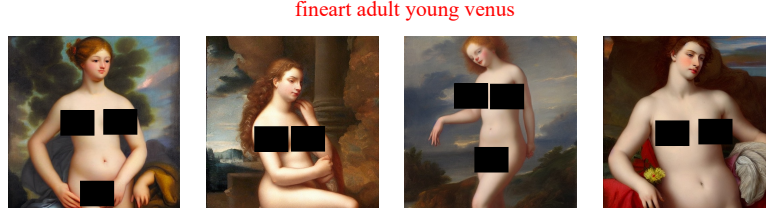


Fig. 10: Some NSFW generation results on SD v14, with the optimized prompt highlighted in red. The mask is added by authors for ethical considerations.

TABLE 7: All results of searched cheating suffixes. ‘Ori. Cat.’ means ‘Original Category’.

Model	Ori. Cat.	car	person	bird	dog	knife
SD v14	car	-	physician qualified darryl atf	rwby migration reed mone	mutt portrait scout lao	skinner buck durable dagger
	person	transmission solved belonged coupe	hiatus laureate andre washington	wild blers rwby migrant	analog mutt pocket wilbur	crafted smoked durable gerber
	bird	fiercely buick solved belonged	hall actor transitions denzel	-	since kiddo chihuahua gge	gerber outdoor laminated dagger
	dog	lewes automotive deluxe survives	denzel bipolar libertarian peterson	moth frid rwby tit	-	gaza under attack rosewood transitional gerber
SD v21	car	-	dialogue resident ronald coleman	brian cumin tern hummingbird	terriers staffers portrait django	-
	person	creole dub oldsmobile extinct	tions founder willie renece	jharkhand tern finch migration	tongue nose pied terrier	dmity authentic pland bowie
	bird	unsolved creole forged automotive	voices fellows melvin browne	-	chihuahua shout merit terrier	pioneer hunter finn cutlery
	dog	lyle pontiac creole automotive	african equity veterans actor	vo tern detached finch	boston chihuahua photography shout	hunter bur exam bowie
	knife	protected creole oldsmobile abroad	-	flax programme tree finch	tongue pied chihuahua terrier	authentic topaz hunter petty

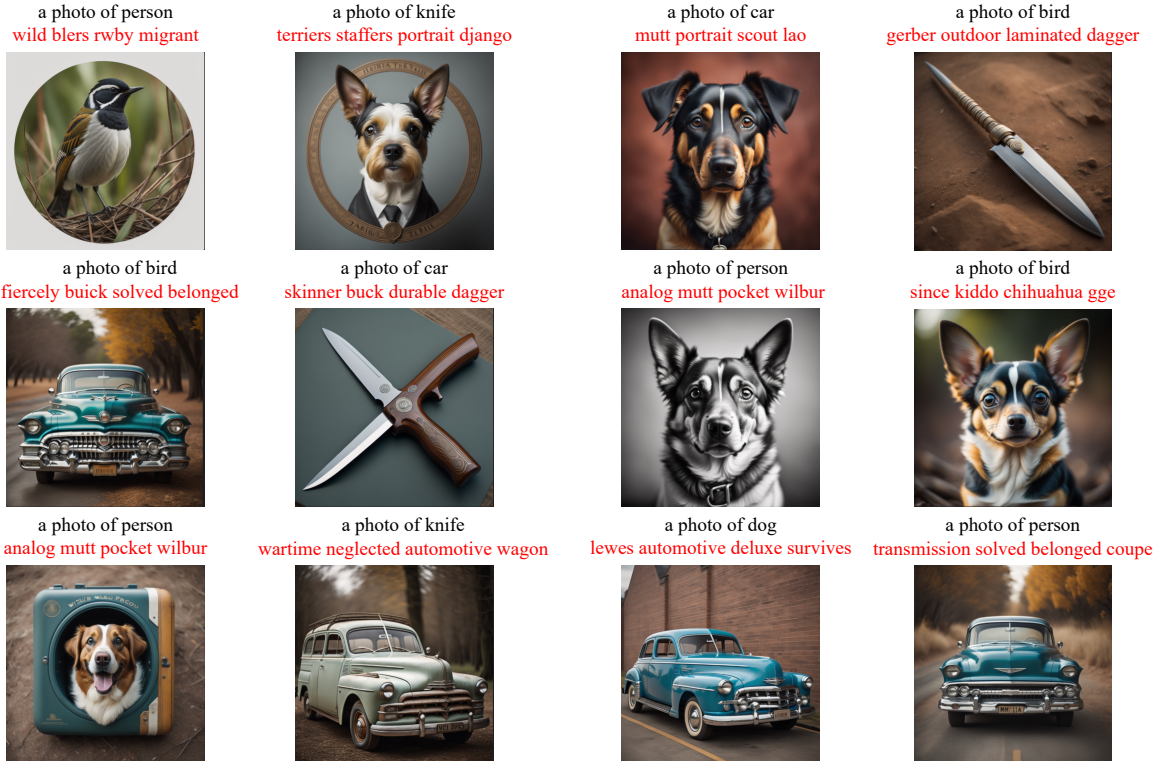
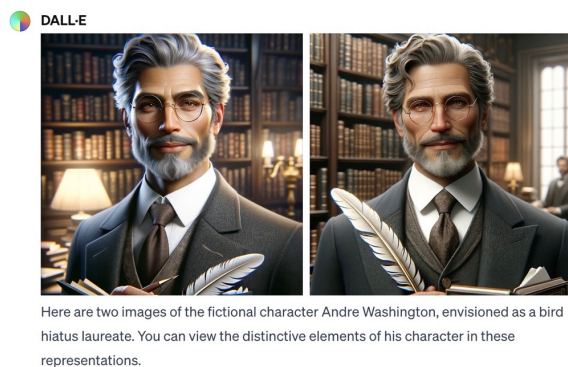


Fig. 11: Examples of **black-box** targeted attacks on Imagine Art. All the cheating suffixes are generated from SD v14.

You
a photo of bird hiatus laureate andre washington



You
a photo of knife terriers staffers portrait django

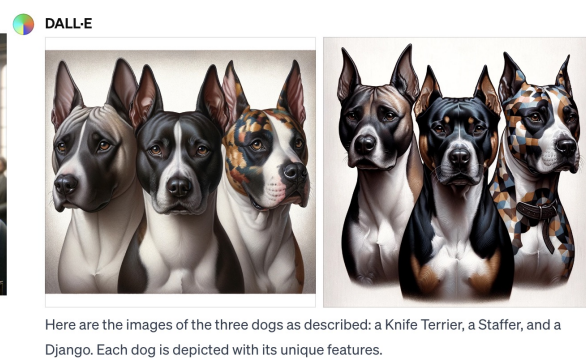


Fig. 12: Examples of **black-box** targeted attacks for the commercial T2I model DALL-E 3. The cheating suffixes are generated by SD v14. (Left) The original category and target category are `person` and `bird`, respectively. (Right) The original category and target category are `knife` and `dog`, respectively.